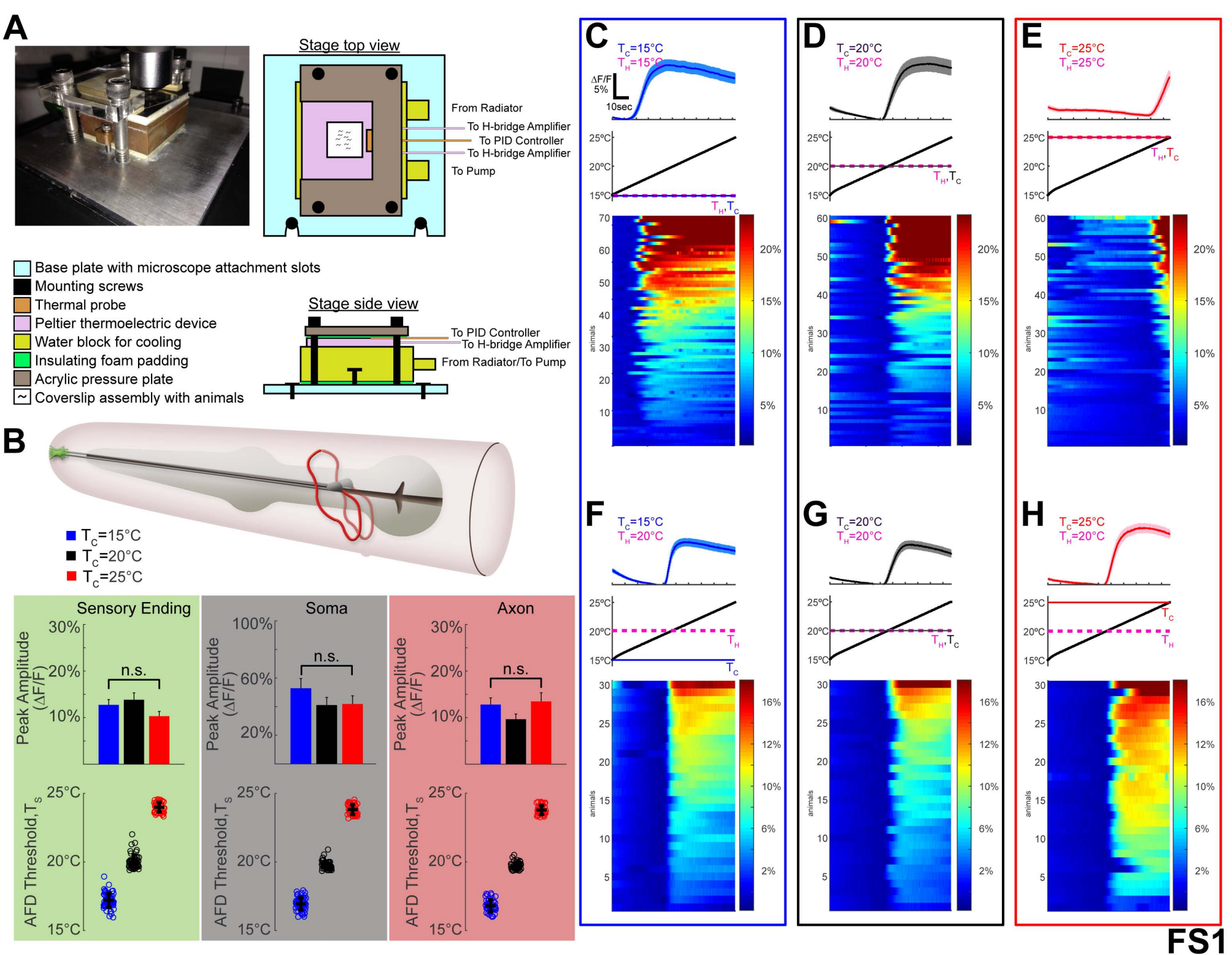
A
Stage top view
From Radiator
To H-bridge Amplifier
To PID Controller
To H-bridge Amplifier
To Pump
Base plate with microscope attachment slots
Mounting screws
Thermal probe
Peltier thermoelectric device
Water block for cooling
Insulating foam padding
Acrylic pressure plate
Coverslip assembly with animals
Stage side view
To PID Controller
To H-bridge Amplifier
From Radiator/To Pump
B
T_C=15°C
T_C=20°C
T_C=25°C
Sensory Ending
Soma
Axon
Peak Amplitude (ΔF/F)
AFD Threshold, T_S
n.s.
C
D
E
F
G
H
T_C=15°C
T_H=15°C
T_C=20°C
T_H=20°C
T_C=25°C
T_H=25°C
T_H=20°C
ΔF/F 5%
10sec
animals
FS1

Figure S1. AFD thermosensory responses adapt rapidly. Related to Figure 1. (**A**) Picture and schematic of the thermoelectric control system used for calcium imaging. Animals immobilized by levamisole were mounted on an agarose pad between two coverslips and placed directly onto the thermoelectric device. Precise temperature control at the peltier surface is achieved via a proportional-integral-derivative (PID) controller (Accuthermo) that gates applied current via an H-bridge amplifier (Accuthermo). A water-cooling system extracts excess heat, as represented in the schematic. Specific temperature protocols were supplied to the PID controller through a custom computer interface written in LabView (see Methods for additional information). (**B**) AFD thermosensory response properties are similar in different subcellular compartments of the AFD neuron. At top, an illustration of AFD morphology highlighting the regions analyzed. The sensory ending is pseudocolored in green, the soma in gray, and the axon in red (modified from WormAtlas). In the graphs at the bottom of the figure, we similarly color the background of the graphs to correspond to the subcellular regions tested. The peak response amplitude (top panel bar graphs) and AFD response threshold (bottom panel dot graphs) were analyzed in animals trained T_C=15°C (blue), T_C=20°C (black)**,** or T_C=25°C (red) for each of these regions. Note that the different training conditions did not produce significant differences in response amplitude between regions tested. Response thresholds were similar in all three regions and distinct between training conditions. (**C-E**) Calcium imaging of AFD responses to a rising linear ramp of 0.1°C/sec from 15°C to 25°C on animals trained at T_C=15°C in **C**, T_C=20°C in **D**, or T_C=25°C in **E**. Mean responses (top panel), stimulus ramp (middle panel), and heat maps (bottom panel) are shown for each condition. Mean responses (dark lines) are illustrated with standard error represented by lighter shaded areas. Heat maps (bottom panel) illustrate the individual responses from >60 animals (each animal is a row) through time. Because of the large sample size in these panels and the variance in AFD response amplitude, some samples are illustrated as saturated signals to allow the frequency of response to be apparent in the heat map. Note that AFD thermosensory responses occur at a threshold temperature (T_S) that adapts with experience for animals raised at T_C=15°C (T_S=16.9°C+/-0.5°C) in **C**, for animals raised at T_C=20°C (T_S=19.8°C+/-0.5°C) in **D**, and for animals raised at T_C=25°C (T_S=23.9°C+/-0.4°C) in **E**. The data shown here correspond to that of **Figure 1E**. (**F-H**) Like **C-E**, but after 30min of adaptation at 20°C (T_H=20°C) as described in **Figure 1A**. Note that after 30min of T_H=20°C, animals previously trained at T_C=15°C, 20°C or 25°C show a response threshold very near T_H and not T_C (T_S=19.5°C+/-0.1°C; T_S=19.9°C+/-0.2°C and T_S=20.1°C+/-0.4°C respectively). The data shown here correspond to that of **Figure 1I**.

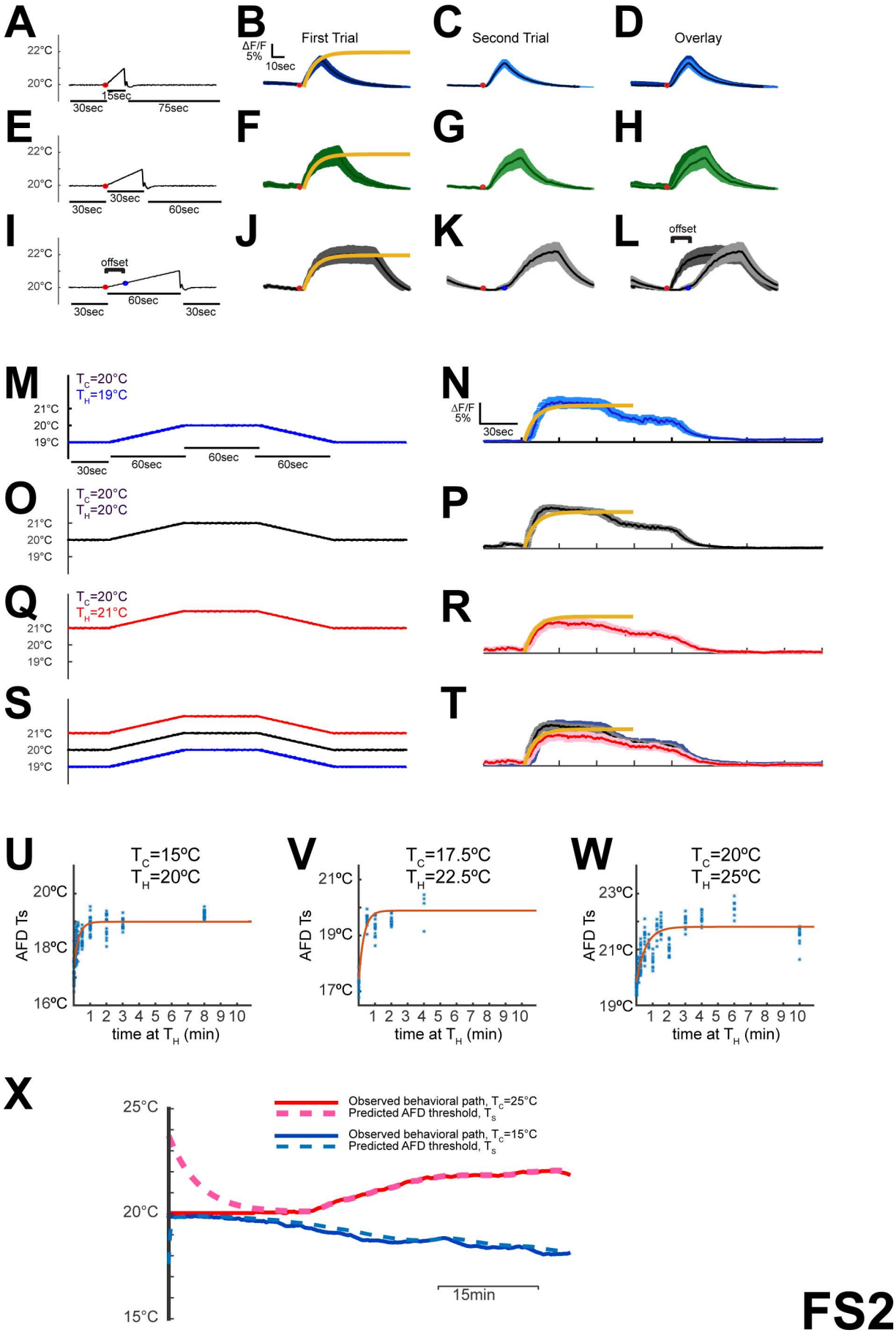
A
22°C
20°C
15sec
30sec
75sec
B
First Trial
ΔF/F
5%
10sec
C
Second Trial
D
Overlay
E
22°C
20°C
30sec
30sec
60sec
F
G
H
I
22°C
20°C
offset
60sec
30sec
30sec
J
K
L
offset
M
T_C=20°C
T_H=19°C
21°C
20°C
19°C
30sec
60sec
60sec
60sec
N
ΔF/F
5%
30sec
O
T_C=20°C
T_H=20°C
21°C
20°C
19°C
P
Q
T_C=20°C
T_H=21°C
21°C
20°C
19°C
R
S
21°C
20°C
19°C
T
U
T_C=15°C
T_H=20°C
AFD Ts
20°C
18°C
16°C
1 2 3 4 5 6 7 8 9 10
time at T_H (min)
V
T_C=17.5°C
T_H=22.5°C
AFD Ts
21°C
19°C
17°C
1 2 3 4 5 6 7 8 9 10
time at T_H (min)
W
T_C=20°C
T_H=25°C
AFD Ts
23°C
21°C
19°C
1 2 3 4 5 6 7 8 9 10
time at T_H (min)
X
25°C
20°C
15°C
Observed behavioral path, T_C=25°C
Predicted AFD threshold, T_S
Observed behavioral path, T_C=15°C
Predicted AFD threshold, T_S
15min

FS2

Figure S2. AFD thermosensory responses encode variations in temperature. Related to Figure 1. (**A-L**) AFD calcium responses indicate direction and duration of temperature change. Animals held at the cultivation temperature (T_C=20°C) were then exposed to a defined thermal ramp of 1°C over 15sec in **A-D** (n=10), 30sec in **E-H** (n=8), or 60sec in **I-L** (n=11). Stimulus onset is marked with a red dot. For each stimulus protocol in **A, E,** and **I**, two immediately consecutive tests were performed on the same animals (first response in **B, F** and **J** and second response in **C, G** and **K**). An overlay of the two consecutive responses are shown in **D, H** and **L**. The AFD calcium rise fits a single exponential function related to the duration of ramping stimulus ($y=C*(1-e^{-kt})$, yellow curve in **B**, **F** and **J**). Note that while overlay of first and second responses fit well in **D** and **H,** we observed a shift in the response timing ("offset") of the second response with a 60sec stimulus in **I**, as illustrated in the overlay, **L**. The observed shift for this 60sec ramp is consistent with the rapid adaptation kinetics of the AFD threshold (**Figure 1J**), and suggest that the shift is due to adaptation experienced by the animal during the 60sec test stimulus of the first trial in **J**. (**M-T**) AFD responds to changes in temperature independently of absolute temperature, consistent with previous observations (Clark et al., 2006; Kimura et al., 2004) and independent of cultivation temperature memory. Animals cultivated at T_C=20°C were held for 30min at T_H=19°C in **N** (n=29), 20°C in **P** (n=26), or 21°C in **R** (n=24), and then subjected to the protocols in **M, O** and **Q**. An overlay of these responses in **T** illustrates that AFD responds similarly regardless of holding temperatures, and that the rising phase of the response fits an exponential function (yellow curve in **T**, identical to curves in **B, F**, **J, N, P**, and **R**). (**U-W**) AFD thermosensory thresholds adapt within minutes to new holding temperatures. Animals trained at T_C=15°C in **U** (n=269 total animals examined, with each dot representing a measurement from a single animal. 17-44 animals were examined for each timepoint, for a total of 9 timepoints as indicated in the graph), T_C=17.5°C in **V** (n=75 with 7-15 animals examined for each timepoint, for a total of 6 timepoints as indicated in the graph), or T_C=20°C in **W** (n=233 with 8-37 animals examined for each timepoint, for a total of 14 timepoints as indicated in the graph) were then shifted to a holding temperature ($T_H=T_C$+5°C) for defined durations of time (as indicated in the graph) to assess AFD sensory adaptation dynamics. The threshold temperature of AFD response (T_S) is plotted as a function of the time held at the new temperature (T_H=20°C). Note that similarly rapid adaptation kinetics were observed regardless of the initial T_C. AFD adaptation with these temperature shifts can be adequately modeled with a single exponential function. Adaptation over larger temperature shifts have been previously shown to fit a double exponential function, suggesting different adaptation kinetics and mechanisms depending on magnitude of temperature shift and time (Yu et al., 2014). (**X**) Based on the kinetics we uncovered for AFD adaptation (**Figure 1J** & **Figure S1U-W**), we modeled AFD adaptation during behavior. The observed migratory route of a single worm with T_C=15°C (blue solid line) or T_C=25°C (red solid line) is illustrated over a 60min thermotaxis behavioral run. Using an exponential function, we calculated the predicted AFD threshold value, T_S, at each time point based on the current temperature and previous T_S value as illustrated by the dashed light blue (T_C=15°C) and light red (T_C=25°C) lines (further explained in Methods). Note that AFD adapts such that during migration, the threshold closely mirrors current temperature on a

migratory path. Note also that animals trained at 25°C (T_c) display an initial delay in the AFD adaptation kinetics not observed for animals trained at 15°C. We propose this delayed adaptation is the reason why animals trained at 25°C (T_c) display a delay in thermotaxis performance as compared to animals trained at 15°C (Ito et al., 2006).

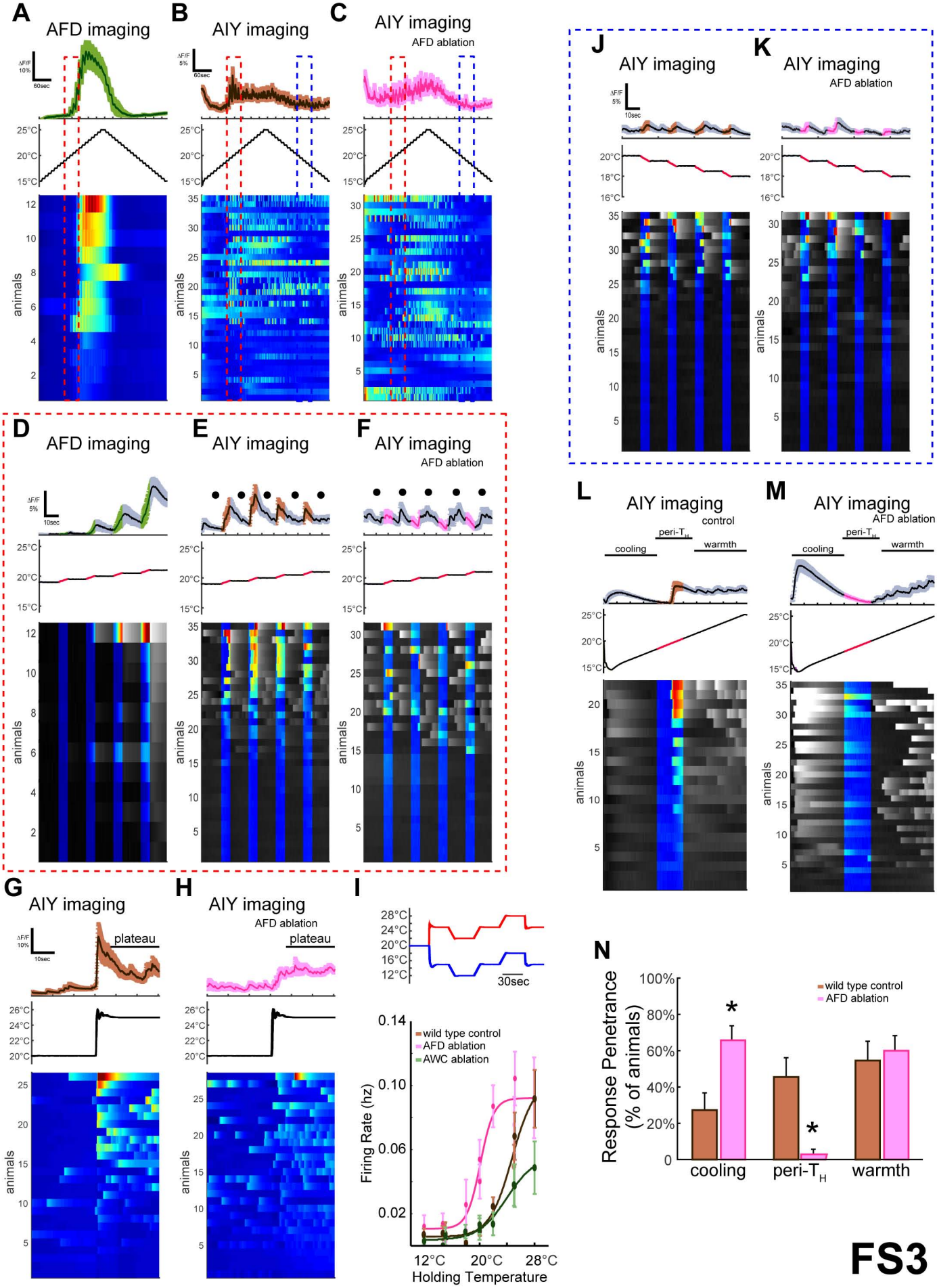
A
AFD imaging
B
AIY imaging
C
AIY imaging
AFD ablation
J
AIY imaging
K
AIY imaging
AFD ablation
D
AFD imaging
E
AIY imaging
F
AIY imaging
AFD ablation
L
AIY imaging
control
cooling
peri-T$_H$
warmth
M
AIY imaging
AFD ablation
cooling
peri-T$_H$
warmth
G
AIY imaging
plateau
H
AIY imaging
AFD ablation
plateau
I
30sec
wild type control
AFD ablation
AWC ablation
Firing Rate (hz)
Holding Temperature
12°C
20°C
28°C
N
Response Penetrance (% of animals)
wild type control
AFD ablation
cooling
peri-T$_H$
warmth
animals
FS3

Figure S3. AIYs display distinct AFD-dependent and AFD-independent temperature responses. **Related to Figure 2**. (**A-C**) AFD in **A** and postsynaptic AIY in **B, C** calcium responses to thermal staircase protocol in wild type in **A, B** or AFD-ablated in **C** animals. In all panels, animals expressing GCaMP6 cell-specifically in AFD in **A** or AIY in **B, C** were trained at T_C=20°C, anesthetized as described in Methods and examined at T_H=20°C. Note that AFD responds only above a threshold near T_H (red dashed box) during the rising phase of the staircase protocol in **A**. AIY displays a complex pattern of responses to the staircase protocol, including synchronized responses on the ramping phase near the holding temperature (red dashed box in **B**). Cell-specific ablation of AFD alters the responses in AIY, most notably by eliminating the peri-T_H ramping response (red dashed box in **C**). (**D-F**) To highlight the responses eliminated by AFD ablation, the data from **A-C** are illustrated at higher magnification and ordered based on the magnitude of response during the peri-T_H ramping phase (red dashed box in **A-C**). In the top row, which represent the mean fluorescent traces for responses in AFD in **D** or AIY in **E, F** for the indicated stimuli (middle row), the plateau periods between temperature steps are in grayscale (and highlighted with black dots), whereas ramping periods are highlighted in color. Similarly, in the stimuli protocol schematized in the middle panels, ramps are highlighted in red and plateaus in black. Note that the onset of AFD response occurs during this ramping phase and at the temperature ramps in **A**, **D**, and that the AIY synchronized responses are also predominantly occurring at the temperature ramps in **E** (highlighted in brown in top panel; also highlighted in color in the calcium heat maps for individual animals in lower panels). Ablation of AFD does not eliminate all of AIY responses, but does abrogate the observed synchronized responses during the temperature ramps (brown in **E** and red in **F** upper panels). Note also the emergence of ectopic response peaks during the plateau phases in the AIY responses of AFD ablated animals (black dots in mean trace of the upper panels of **F**). (**G-I**) Examination of AFD-independent plateau responses to temperature in AIY. Animals T_C=20°C;T_H=20°C were exposed to a single temperature step to 25°C and calcium responses were recorded in AIY for wild type in **G** and AFD-ablated in **H** animals. Note that the temperature increase elicits a synchronized response to temperature during the ramping phase in **G** and that this response is AFD-dependent in **H**. Also note that the synchronized response is followed by a period of calcium responses to the plateau period in which animals are held at the new temperature. Consistent with observations using protocols in **F**, these responses in AIY during the temperature plateau are not eliminated upon ablation of AFD in **H**. (**I**) Animals trained at T_C=20°C; T_H=20°C were subjected to one of the two protocols (red or blue) schematized in **I** (top panel). In these two protocols, animals are exposed to 30-sec holds either above (red) or below (blue) T_H as illustrated. Responses of mean firing frequency as a function of plateau temperature reveals a sigmoidal response curve with increased firing frequency in wild-type N2 worms above 20°C (brown curve, 26 animals were examined for each of the two protocols, for a total of 52 animals). In animals with AFD ablated (pink curve, n=28 animals were examined for the protocol above T_H and n=29 animals were examined for the protocol below T_H), AIY responses during plateau periods are still observed with response frequency rising at lower temperatures than observed in control animals.

These data suggest that the AIY plateau responses are not dependent on AFD, but are modulated by AFD. In contrast, ablation of the olfactory neuron AWC (Beverly et al., 2011) significantly reduces this AIY plateau response at higher temperatures. These data are consistent with reports that AWC displays stochastically timed responses to warm temperatures (Beverly et al., 2011; Biron et al., 2008; Kuhara et al., 2008), and suggests that these AWC responses contribute to the observed, AFD-independent temperature responses in AIY (Ohnishi et al., 2011). **(J)** AIY also responds to temperature decrements as shown below 20°C of the staircase protocol from **A-C** (blue dashed box). (**K**) In animals with AFD ablated, AIY response peaks are still observed during temperature decrements below 20°C, indicating that these responses can occur without AFD. (**L**) In worms with T_C=20°C and T_H=20°C, a single temperature decrement to 15°C followed by a linear ramp of 0.1°C/sec to 25°C illustrates responses to all three elements of the temperature protocol: decrement below 20°C ("cooling", grayscale), warming near 20°C ("peri-T_H", color), and temperatures above 20°C ("warmth", grayscale). (**M**) This protocol further illustrates that only the peri-T_H warming response is eliminated with AFD ablation, but that other responses can be modulated by AFD. (**N**) Upon AFD ablation (pink), the percentage of animals observed to have an AIY calcium response ("penetrance") selectively decreases during the peri-T_H window. Thus, AIY response frequency in the peri-T_H window is AFD dependent. Interestingly, a higher response penetrance can be noted in the cooling response after AFD ablation, consistent with AFD playing modulatory roles in these other temperature responses, similar to its modulatory role in the plateau responses to warming temperatures in **I**. * indicates $p<0.05$.

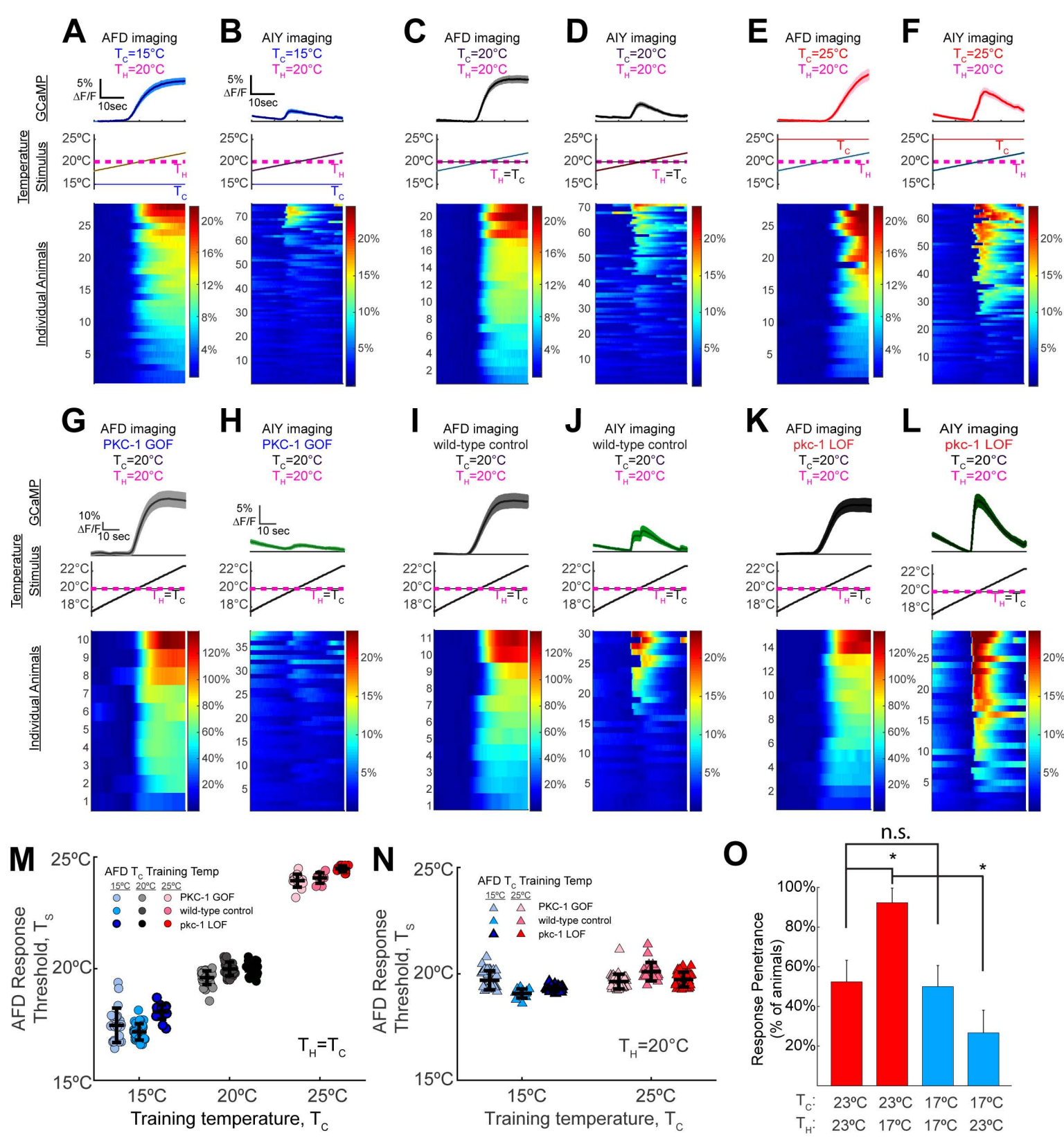
A
AFD imaging
T_C=15°C
T_H=20°C
B
AIY imaging
T_C=15°C
T_H=20°C
C
AFD imaging
T_C=20°C
T_H=20°C
D
AIY imaging
T_C=20°C
T_H=20°C
E
AFD imaging
T_C=25°C
T_H=20°C
F
AIY imaging
T_C=25°C
T_H=20°C
GCaMP
5% ΔF/F
10sec
Temperature Stimulus
25°C
20°C
15°C
T_H
T_C
T_H=T_C
Individual Animals
G
AFD imaging
PKC-1 GOF
T_C=20°C
T_H=20°C
H
AIY imaging
PKC-1 GOF
T_C=20°C
T_H=20°C
I
AFD imaging
wild-type control
T_C=20°C
T_H=20°C
J
AIY imaging
wild-type control
T_C=20°C
T_H=20°C
K
AFD imaging
pkc-1 LOF
T_C=20°C
T_H=20°C
L
AIY imaging
pkc-1 LOF
T_C=20°C
T_H=20°C
10% ΔF/F
10 sec
22°C
20°C
18°C
M
AFD T_C Training Temp
15°C 20°C 25°C
PKC-1 GOF
wild-type control
pkc-1 LOF
AFD Response Threshold, T_S
T_H=T_C
Training temperature, T_C
N
AFD T_C Training Temp
15°C 25°C
PKC-1 GOF
wild-type control
pkc-1 LOF
AFD Response Threshold, T_S
T_H=20°C
Training temperature, T_C
O
n.s.
*
*
Response Penetrance (% of animals)
100%
80%
60%
40%
20%
T_C: 23°C 23°C 17°C 17°C
T_H: 23°C 17°C 17°C 23°C

FS4

Figure S4. Directed migration on a thermal gradient is associated with changes in post-synaptic responses to AFD rather than changes in AFD sensory function. Related to Figures 2 and 3. (**A-F**) Calcium dynamics of single AFD neurons in **A, C, E** or AIY neurons in **B, D, F** of animals trained at T_C=15°C in **A** and **B**, T_C=20°C in **C** and **D**, or T_C=25°C in **E** and **F,** all with T_H=20°C. Note that while AFD responds robustly in all conditions, the response frequency and amplitude in AIY varies depending on the cultivation temperature memory (see **Figure 2** for quantification). (**G-L**) PKC-1 loss-of-function and gain-of-function mutants in AFD, which produce distinct thermal preference behaviors independent of experience ((Okochi et al., 2005) and **Figure 3A-C**), were cultivated at T_C=20° and examined for calcium responses in AFD neurons in **G**, **I**, **K** or AIY neurons in **H**, **J**, **L**. Note that PKC-1 manipulations in AFD do not impact AFD sensory responses, but instead alter response frequency and amplitude in the postsynaptic partner AIY. Also, these effects phenocopy the changes in AIY response observed with experience in **A**-**F**. (**M**) AFD response thresholds for PKC-1 gain-of-function, wild type or PKC-1 loss-of-function mutants trained at different T_C as indicated in the legend in **M**. Each circle represents the response of a single animal. Note that the AFD response threshold does not significantly change across genotypes, but varies based on T_H (which, in this particular experiment, T_H=T_C). (**N**) From T_C=15°C (blue) or T_C=25°C (red), animals were then held at T_H=20°C for 30min. For all three genotypes, T_S values adapted to nearly 20°C within this period. Together, these findings indicate that AFD response thresholds and adaptability are not impacted by in PKC-1 GOF or LOF mutants. (**O**) To address whether the change in AIY response frequency was a consequence of absolute temperature versus the relationship between the training temperature, T_C, and the testing temperature, T_H, we trained animals at either T_C=23°C (red) or T_C=17°C (blue), then assayed AIY response frequency for 4 groups: T_C=23°C/T_H=23°C, T_C=23°C/T_H=17°C, T_C=17°C/T_H=17°C, T_C=17°C/T_H=23°C. We observed that the AIY response frequency was ~50% when T_C=T_H, irrespective of the absolute value of the temperature (compare T_C=23°C/T_H=23°C and T_C=17°C/T_H=17°C. Also observed for T_C=20°C/T_H=20°C in Figure 2H). We also observed that when T_C>T_H, the AIY response frequency was enhanced with respect to T_C=T_H or T_C<T_H. Together, our findings indicate that the change in AIY response frequency is a consequence of the relationship between the training temperature, T_C, and the testing temperature, T_H. * indicates $p<0.05$ in Fisher's Exact test. Error bars denote SEM.

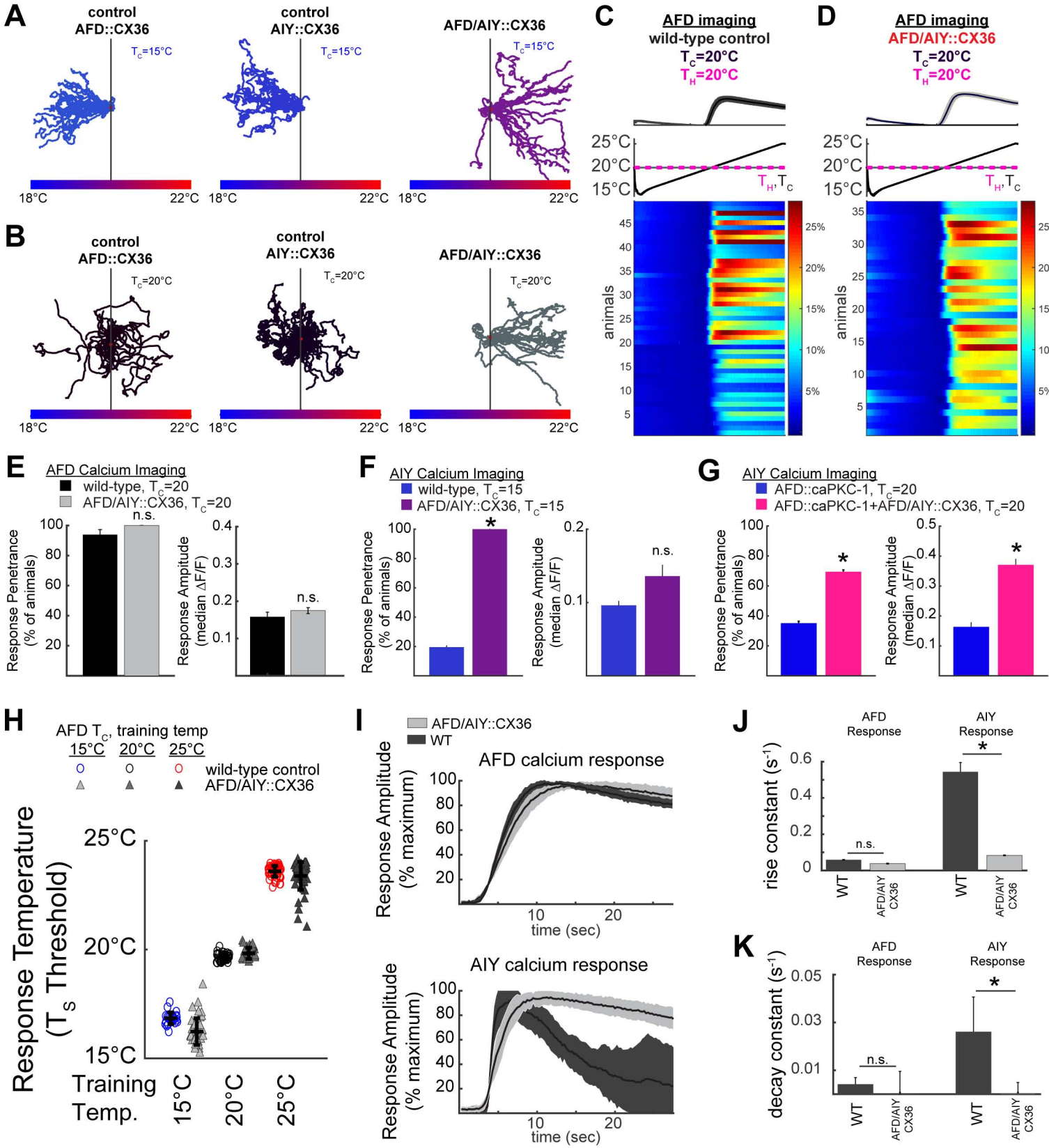
A
control AFD::CX36
control AIY::CX36
AFD/AIY::CX36
T_C=15°C
18°C
22°C
B
control AFD::CX36
control AIY::CX36
AFD/AIY::CX36
T_C=20°C
18°C
22°C
C
AFD imaging
wild-type control
T_C=20°C
T_H=20°C
25°C
20°C
15°C
T_H,T_C
animals
25%
20%
15%
10%
5%
D
AFD imaging
AFD/AIY::CX36
T_C=20°C
T_H=20°C
E
AFD Calcium Imaging
wild-type, T_C=20
AFD/AIY::CX36, T_C=20
n.s.
Response Penetrance (% of animals)
Response Amplitude (median ΔF/F)
F
AIY Calcium Imaging
wild-type, T_C=15
AFD/AIY::CX36, T_C=15
*
n.s.
G
AIY Calcium Imaging
AFD::caPKC-1, T_C=20
AFD::caPKC-1+AFD/AIY::CX36, T_C=20
H
AFD T_C, training temp
15°C 20°C 25°C
wild-type control
AFD/AIY::CX36
Response Temperature (T_s Threshold)
Training Temp.
I
AFD/AIY::CX36
WT
AFD calcium response
AIY calcium response
Response Amplitude (% maximum)
time (sec)
J
AFD Response
AIY Response
rise constant (s^-1)
WT
AFD/AIY CX36
K
decay constant (s^-1)

FS5

Figure S5. CX36 behavioral phenotype is not a consequence of hemi-channel formation or altered AFD sensory function. Related to Figure 5. (**A**) Stable, integrated lines expressing CX36 in individual AFD (left panel) or AIY (middle panel) neurons were created and then examined in thermotaxis behavior. Note that expression of the CX36 hemichannel in either AFD (AFD::CX36) or AIY (AIY::CX36) does not affect thermotaxis behavior for animals with T_C=15°C (n=25 for each experiment), consistent with the study by (Rabinowitch et al., 2014), which shows that expression of just CX36 hemichannels do not have a detectable behavioral consequence in *C. elegans* neurons. These studies are also consistent with gap junction studies that demonstrate that vertebrate connexins do not interact with invertebrate innexins (Epstein and Gilula, 1977). Crossing these integrated lines to each other yields animals expressing CX36 in both AFD and AIY (AFD/AIY::CX36), expected to form a synthetic gap junction between AFD and AIY. These animals display a strong bias toward the warm side of the gradient (right panel). This same line was analyzed in **Figure 5 B, D**. (**B**) Similar to **A**, but with animals trained at T_C=20°C (n=25 for each experiment) (**C-D**) Calcium imaging in AFD of wild type animals in **C** and AFD/AIY::CX36 animals in **D**. Note that the AFD/AIY::CX36 does not alter AFD response properties as assessed by calcium imaging. (**E**) Quantification of **C** and **D** shows that both wild-type (WT) and AFD/AIY::CX36 animals display high penetrance of temperature responses in AFD (left panel) and similar response amplitudes (right panel). (**F**) Quantification of **Figure 5 A, B** shows that the integrated AFD/AIY::CX36 animals have a significant increase in response frequency in AIY compared to control animals cultivated at T_C=15°C. (**G**) Quantification of **Figure 5 E, F** shows that expression of AFD/AIY::CX36 through an extrachromosomal transgenic array enhances response penetrance in worms that are also expressing the AFD::caPKC-1 transgene. (**H**) Wild-type animals trained at T_C=15°C (blue), T_C=20°C, or T_C=25°C show distinct AFD response thresholds that are not affected in AFD/AIY::CX36 animals (gray). (**I**) Expression of the vertebrate gap junction protein CX36 in AFD and AIY (AFD/AIY::CX36) creates a strong positive coupling between AFD and AIY. The responses of AFD (top panel) and AIY (bottom panel) to a warming stimulus (0.1°C /sec) were normalized to the maximum signal per response for analyses of kinetics. AFD/AIY::CX36 (light gray) did not alter the kinetics of AFD thermal responses (top panel). A similar analysis of AIY thermal responses shows a clear change in AIY response kinetics (bottom panel) in AFD/AIY::CX36 animals (light gray) in comparison to wild-type animals (dark gray). (**J,K**) In AFD/AIY::CX36 animals, AIY responses match the kinetics of AFD rather than those of wild-type AIY, as shown by the quantification of constants after exponential fitting for the calcium transient rise in **J** and decay in **K**. The change in AIY response kinetics in AFD/AIY::CX36 animals as compared to the AIY kinetics in wild type animals, and the fact that the AIY kinetics in those animals is indistinguishable from the AFD kinetics, suggest a strong electrical coupling between AFD and AIY, consistent with an ectopic gap junction. * indicates $p<0.05$ in Mann-Whitney-Wilcoxon test for amplitude data and Fisher's Exact test for penetrance data. Error bars denote SEM.